

# A series of five population-specific Indian brain templates and atlases spanning ages 6 to 60 years

## Authors:

Bharath Holla<sup>1\*#</sup>, Paul A. Taylor<sup>2#</sup>, Daniel R. Glen<sup>2</sup>, John A. Lee<sup>2</sup>, Nilakshi Vaidya<sup>1,8</sup>, Ur-  
vakhsh Meherwan Mehta<sup>1</sup>, Ganesan Venkatasubramanian<sup>1</sup>, Pramod Pal<sup>1</sup>, Jitender Saini<sup>1</sup>, Naren P.  
Rao<sup>1</sup>, Chirag Ahuja<sup>3</sup>, Rebecca Kuriyan<sup>4</sup>, Murali Krishna<sup>5</sup>, Debashish Basu<sup>3</sup>, Kartik Kalyanram<sup>6</sup>,  
Amit Chakrabarti<sup>7</sup>, Dimitri Papadopoulos Orfanos<sup>8</sup>, Gareth J. Barker<sup>9</sup>, Robert W. Cox<sup>2</sup>, Gunter  
Schumann<sup>10</sup>, Rose Dawn Bharath<sup>1\*</sup>, Vivek Benegal<sup>1</sup>

## Affiliations:

<sup>1</sup>National Institute of Mental Health and Neuro Sciences, Bengaluru, India; <sup>2</sup>Scientific and Sta-  
tistical Computing Core, NIMH, NIH, Bethesda, MD, USA; <sup>3</sup>Post Graduate Institute of Medical  
Education and Research, Chandigarh, India; <sup>4</sup>St. John's Medical College and Research Institute,  
Bengaluru, India; <sup>5</sup>CSI Holdsworth Memorial Hospital, Mysore, India; Foundation for Research and  
Advocacy in Mental Health, Mysore, India; <sup>6</sup>Rishi Valley Rural Health Centre, Madanapalle, AP,  
India; <sup>7</sup>ICMR-Regional Occupational Health Centre, Kolkata, India; <sup>8</sup>NeuroSpin, CEA, Université  
Paris-Saclay, Paris, France; <sup>9</sup>Institute of Psychiatry, Psychology and Neuroscience (IoPPN), King's  
College London (KCL), UK; <sup>10</sup>Centre for Population Neuroscience and Stratified Medicine (PONS),  
SGDP Centre, IoPPN, KCL, UK; Institute of Science and Technology, Fudan University, Shanghai,  
PRC; Department of Psychiatry and Psychotherapy, Charite, Universitaetsmedizin Berlin-Mitte,  
Humboldt University, Berlin, Germany.

## \*Corresponding Authors:

Bharath Holla ([hollabharath@gmail.com](mailto:hollabharath@gmail.com)); Rose Dawn Bharath ([drrosedawnbharath@gmail.com](mailto:drrosedawnbharath@gmail.com))

#Equally contributing authors.

## Abstract

Anatomical brain templates are commonly used as references in neurological MRI studies, for bringing data into a common space for group level statistics and coordinate reporting. Having a group representative template increases the accuracy of alignment, improves statistics and decreases distortions (as well as potential biases) in final coordinate reports. Given the inherent variability in brain morphology across age and geography, it is important to have templates that are as representative as possible for both age and population. In this study, we developed and validated a new set of T1w Indian brain templates (IBT) from a large number of subjects (total n=466) across different Indian states and acquired at multiple 3T MRI sites. A new tool in AFNI, `make_template_dask.py`, which uses the Dask python parallelization library, was created to efficiently make a template from a group of subjects. A total of five age-specific

35 categories of IBTs [ages 6-11 yrs (C1), 12-18 yrs (C2), 19-25 yrs (C3), 26-40 yrs (C4), and  
36 41-60 yrs (C5)], as well as maximum probability map (MPM) atlases for each template were  
37 generated; for each age group's template-atlas pair, there is both a "population average" and a  
38 "typical" version. Validation experiments on an independent Indian structural and functional  
39 MRI dataset show the appropriateness of IBTs for spatial normalization of Indian brains. The  
40 results indicate significant structural differences when comparing the IBTs and MNI template,  
41 with these differences being maximal along the Anterior-Posterior and Inferior-Superior axes,  
42 but minimal Left-Right. For each age group, the MPM brain atlases provide reasonably good  
43 representation of the native-space volumes in the IBT space, except in a few regions with high  
44 inter-subject variability as indicated by high mean deformation value. These findings provide  
45 evidence to support the use of age and population-specific templates in human brain mapping  
46 studies. These templates, with corresponding atlases and tools, are publicly available on the  
47 NIMHANS and AFNI websites.

48 **Keywords:** MRI, brain template, brain atlases, maximum probability map

## 49 1 Introduction

50 The shape, size and volume of the human brain is highly variable across individuals, as well as across  
51 age, gender and geographical location or ethnicity. This fact is of prime importance in neuroimaging  
52 group studies, where the brains of all subjects are typically aligned to a single template space for  
53 data analysis and for the reporting of findings where analogous anatomical structures are mapped  
54 on to the same coordinate location across the subjects. A brain template provides a standard  
55 3D coordinate frame to combine and/or compare data from many subjects, across different imaging  
56 modalities, structural or functional and even different laboratories around the world. The properties  
57 of the template (size, shape, tissue contrast, etc.) directly affect the quality of alignment.

58 An early brain atlas was constructed by [Talairach and Tournoux \[1988\]](#) from a post mortem brain  
59 of one 60-year-old French woman, introducing the concepts of coordinate system and spatial trans-  
60 formation to brain imaging. However, using a single subject brain as a template introduces several  
61 idiosyncrasies, as it does not account for groupwide anatomical variability, asymmetry, age-related  
62 differences, etc. In order to address some of these issues, a subsequent initiative from the Montreal  
63 Neurological Institute (MNI) resulted in a statistical brain template (MNI-305) using 305 young  
64 right-handed subjects [[Evans et al., 1993](#)]. While this composite template better accounted for  
65 anatomical variability, it also had relatively low tissue contrast and structural definition, which  
66 can affect the ability of alignment algorithms to provide high quality anatomical matching across a  
67 group study. In 2001, the international consortium for human brain mapping (ICBM) introduced  
68 the revised MNI-152 template [[Mazziotta et al., 2001b](#)] with better contrast and structure defini-

69 tion, where 152 individual brains were linearly registered to MNI305 to make an average template.  
70 The ICBM-452 template [Mazziotta et al., 2001a] included all three sites of ICBM and provided  
71 even better signal-to-noise ratio due to the nearly threefold increase in the number of subjects.  
72 These MNI templates were widely adopted by several image processing pipelines, with the asso-  
73 ciated set of coordinates known as “MNI space”. Furthermore, an unbiased non-linear average of  
74 the adult MNI152 and a pediatric template with 20-40 iterative non-linear averages has also been  
75 made available [Fonov et al., 2011]. These templates provide the advantages of retaining group  
76 representativeness of the MNI305 or MNI152 while still providing the details that are closer to  
77 those apparent in a single subject; however, their “representativeness” is limited to a fairly isolated  
78 geographic location and (typically, Western) population, even though neuroimaging studies draw  
79 from populations across the globe.

80 More recently, several research groups around the world have developed and validated brain tem-  
81 plates that are representative of their (broadly) local population. Lee et al. [2005] created a set  
82 of Korean Brain templates with 78 subjects in an age range between 18 to 77 years (young tem-  
83 plate <55 years and elderly template >55 years). Additionally, Tang et al. [2010] generated a  
84 Chinese brain template of 56 subjects (mean age 24.4 years). In each case the groups demonstrated  
85 significantly reduced warp deformations and increased registration accuracy when applying these  
86 templates to studies of local populations. It should be noted that even though the templates draw  
87 from subjects within a population, there is still a large amount of inherent variability evident in the  
88 brain morphology, due to combinations of factors such as inherent structural variability, multi-ethnic  
89 composition and differences in genetic influences and environmental exposures.

90 The benefit of utilizing a population-representative template in the Indian context has also been  
91 recognized, with the additional need for age-specific templates due to the increasingly wide range  
92 of ages enrolled in studies. Recent attempts at developing brain templates for Indian population  
93 have tended to focus on the young adult age group (21-30 years) with relatively small [Rao et al.,  
94 2017] to modest sample sizes [Sivaswamy et al., 2019, Bhalerao et al., 2018, Pai et al., 2020], and  
95 have utilized data from a single site/scanner. Additionally, to date, whole-brain annotated reference  
96 atlases based on segmentation have not accompanied the generated templates. In this study, we  
97 present and validate a new set of brain templates that have been created from a large number  
98 of subjects from multi-site acquisitions across India, with five age ranges provided (between 6-60  
99 years), as well as brain atlases for each template. For each age group’s template-atlas pair, there is  
100 both a “population average” and “typical” version (the latter being the individual brain which most  
101 closely matches the population average, which potentially provides higher detail as an alignment  
102 target and atlas). We present several validation tests for the accuracy and representativeness of the  
103 templates, and we also use data from separately acquired subjects to demonstrate the benefits of  
104 these templates over the existing standard MNI templates for studies on Indian cohorts.

**Table 1** Demographic Profiles.

<b>Age Category</b>	<b>Age Description</b>	<b>Age in years, Mean (Range)</b>	<b>Sample Size N (% Female)</b>	<b>No. States</b>	<b>No. Scanners</b>
C1	Late childhood	9.3 (6 to 11)	28 (46.43%)	5	4
C2	Adolescence	15.1 (12 to 18)	106 (47.17%)	9	5
C3	Young adulthood	21.3 (19 to 25)	181 (40.89%)	15	5
C4	Adulthood	31.1 (26 to 40)	89 (42.7%)	11	2
C5	Late adulthood	52.7 (41 to 60)	62 (43.55%)	6	2

## 105 2 Methods

### 106 2.1 Participants

107 The datasets used in the present study were selected from healthy control subjects from several  
108 imaging studies, across multiple centers and different populations across India. They included  
109 imaging data from the Indian multisite developmental cohort study, the Consortium on Vulnerability  
110 to Externalising Disorders and Addictions (cVEDA) [Sharma et al., 2020, Zhang et al., 2020] and  
111 from stored datasets contributed by researchers at the National Institute of Mental Health and  
112 Neurosciences (NIMHANS, Bengaluru, India). All of these studies were approved by the ethics  
113 review boards at the corresponding participating sites. Inclusion criteria included not having a  
114 personal history of prior brain injury, neurological disorder or psychiatric diagnosis. The sample  
115 was comprised of 466 subjects from a large number of states across India and acquired at multiple  
116 sites. Based on age and demographic distributions, subject datasets were divided into 5 groups:  
117 C1, late childhood (6-11 years); C2, adolescence (12-18 years); C3, young adulthood (19-25 years);  
118 C4, adulthood (26-40 years); C5, late adulthood (41-60 years). The sample size and demographic  
119 information of each cohort is summarized in Table 1.

### 120 2.2 Image acquisition

121 T1-weighted (T1w) three-dimensional high resolution structural brain MRI scans were acquired  
122 from five 3T MRI scanners located at three different locations across India: Bengaluru (site A, C  
123 and D), Mysuru (site B) and Chandigarh (site E). The subjects belonged to several neighboring  
124 states to these locations, with wide geographical representation throughout India. As with most  
125 multisite studies, the acquisition parameters varied slightly across sites and scanners, but were  
126 generally similar, with good grey/white matter contrast with a voxel size close to 1mm isotropic;  
127 details are listed in Table 2.

**Table 2** Acquisition parameters.

Acq Seq	Site label	Scanner model	dx (mm)	dy (mm)	dz (mm)	TR <sup>†</sup> (ms)	TE (ms)	TI (ms)	FA (deg)	Matrix size	No. Sag	No. Subj <sup>‡</sup>
1	A	Achieva <sup>a</sup>	1	1	1	8.2	3.8	745	8	256 × 256	165	50
2	A	Achieva <sup>a</sup>	0.9	0.9	1	8.2	3.8	800	8	257 × 256	160	38
3	B	Ingenia <sup>a</sup>	1.2	1	1	6.9	3.2	725	9	256 × 256	170	29
4	C	Ingenia <sup>a</sup>	1	1	1	6.9	3.3	925	9	256 × 256	211	10
5	D	Skyra <sup>b</sup>	1.2	1	1	2300	3.0	900	9	256 × 240	176	82
6	D	Skyra <sup>b</sup>	1	1	1	1900	2.4	900	9	256 × 256	192	56
7	D	Skyra <sup>b</sup>	0.9	0.9	0.9	1600	2.1	900	9	256 × 256	176	124
8	E	Verio <sup>b</sup>	1.2	0.5	0.5	2300	3.0	900	9	512 × 480	176	77

Acq Seq = acquisition sequence; dx, dy, dz are voxel dimensions; TR = repetition time; TE = echo time; TI = inversion time; FA = flip angle; No. Sag = number of sagittal slices.

<sup>a</sup>Philips, 3T. <sup>b</sup>Siemens, 3T. <sup>‡</sup>This is the final number of subjects included in final templates (total = 466), after all steps of QC and subject removal. <sup>†</sup>The TR for 3D scans such as these is defined differently between Philips and Siemens scanners, with the relationship being  $TR_{\text{Philips}} \approx (TR_{\text{Siemens}} - TI)/(No. Sag)$ .

### 128 2.3 Data Preprocessing and Initial Quality Assurance

129 This processing primarily used programs in the AFNI (v19.0.20) [Cox, 1996] and FreeSurfer (v6.0)  
130 [Fischl, 2012] neuroimaging toolboxes, as well as the “dask” scheduling tool in Python developed by  
131 the Dask Development Team [2016]. Unless otherwise noted, programs named here are contained  
132 within the AFNI distribution. The following processing steps are shown schematically in Figure 1,  
133 in the first column.

134 Datasets were first processed using AFNI’s “fat\_proc\_convert\_dcm\_anat”. Using this, DICOMs  
135 were converted to NIFTI files using dcm2niix\_afni (the AFNI-distributed version of dcm2niix [Li  
136 et al., 2016]). For uniformity and initialization, with this tool, they were also given the same  
137 orientation (RAI), and the physical coordinate origin was placed at the volume’s center of mass (to  
138 simplify later alignments).

139 Next, “fat\_proc\_axialize\_anat” was applied to reduce the variance in the spatial orientation of  
140 brains for later alignment and for practical considerations of further processing steps, as described  
141 here. Each volume was affinely registered to a reference anatomical template (MNI ICBM 152  
142 T1w) that had previously been AC-PC aligned; alignment included an additional weight mask  
143 to emphasize subcortical structure alignment (e.g., AC-PC structures), and only the solid-body  
144 parameters of the alignment were applied, so that no changes in shape were incurred. Because  
145 datasets had been acquired with varied spatial resolution and FOV (see Table 2), the datasets were

146 resampled (using a high-order sinc function, to minimize smoothing) to the grid of the reference  
147 base of 1mm isotropic voxels.

148 All datasets were visually and systematically checked for quality of both data and registration using  
149 the QC image montages that were automatically generated by the previous program. T1w volumes  
150 with noticeable ringing or other artifact (e.g., due to subject motion or dicom reconstruction errors)  
151 were noted and removed from further analyses. T1w volumes with any incidental findings (for  
152 example, large ventricles, cavum septum pellucidum) were also removed.

153 FreeSurfer’s “recon-all” [Fischl, 2012] was run on each T1w data set to estimate surfaces, parcel-  
154 lation and segmentation maps. AFNI’s “@SUMA\_Make\_Spec\_FS” was then run to convert the  
155 FreeSurfer output to NIFTI files and to generate standard meshes of the surface in formats usable  
156 by AFNI and SUMA. Additionally, @SUMA\_Make\_Spec\_FS subdivides the FreeSurfer parcella-  
157 tions into tissue types such as gray matter (GM), white matter (WM), cerebrospinal fluid (CSF),  
158 ventricle, etc. This was followed by visual inspection of parcellation maps overlaid on anatomical  
159 volumes.

160 Next, a whole brain mask of each anatomical volume was created. In several cases, the skullstripped  
161 brain volumes output by recon-all (brain\_mask.nii) included large amounts of non-brain material  
162 (skull, dura, face, etc.), and so an alternative mask was generated using only the ROIs comprising  
163 the parcellation and segmentation maps. For each subject, a whole brain mask was generated by:  
164 first making a preliminary mask from all of the ROIs identified by recon-all; then inflating that pre-  
165 mask by 3 voxels; and finally shrinking the result by two voxels (thus filling in any holes inside the  
166 brain mask and smoothing the outer edges). This produced whole brain masks that were uniformly  
167 specific to each subject’s intracranial volume.

168 Finally, the intensity of tissues within each T1w volume was made uniform with AFNI’s 3dUnifize.  
169 This ensures that each subject’s brain, which had been acquired on different scanners with poten-  
170 tially different scalings, would have equal weight when averaging (e.g., WM is scaled to approxi-  
171 mately a value of 1000 in each brain, and similarly for other tissues), and also reduces the risk of a  
172 bright outlier region driving poor alignment.

## 173 **2.4 Mean template generation**

174 After the above pre-processing steps and QC, the following templatizing algorithm was applied  
175 for each cohort (C1-5) separately. The general procedure was to alternate between alignment to  
176 a reference base (with increasingly higher order of refinement) and averaging the aligned brains  
177 to generate a new reference base for the subsequent iteration. In this way one can generate a

178 cohort mean template of successively greater specificity and detail; after several iterations, the  
179 alignment essentially converges (i.e., additional refinement becomes negligible) and is halted. Warps  
180 were generated and saved at each step. The final nonlinear warps and affine transformations were  
181 concatenated for each subject at the end in order to generate the final group average template.  
182 These steps are also included in the schematic Figure 1, in the first column (bottom) and second  
183 and third columns.

184 The first level of alignment was made from each anatomical in the cohort to the MNI ICBM-152  
185 T1w template using a 6 degree of freedom (DF) rigid body equivalent registration, meaning a full  
186 affine transformation was computed, but only the rigid components were extracted and applied.  
187 The average of all subjects' brains, rigidly aligned to the initial template, was used to create a  
188 single average volume "mean-rigid"; here and at each alignment stage, a cohort standard deviation  
189 map was also created, to highlight locations of relatively high and low variability. That stage's  
190 average volume was then used as a base for the next stage of alignment for each subject, using a 12  
191 DF linear affine registration, and with the results averaged to create the next base "mean-affine".  
192 For these alignments, AFNI's "lpa" cost function (absolute value of local Pearson correlation) [Saad  
193 et al., 2009] was used for high quality alignment of features between volumes of similar contrast.  
194 The cost function computes the absolute value of the Pearson correlation between the volume and  
195 the current template in patches of the volume at a time.

196 As a practical consideration, we note that lower level alignments such as these have a general  
197 property of producing a smoothed brain, which has the additional effect of increasing the apparent  
198 size of the base dataset (i.e., the edge is blurred outward). Therefore, in these initial levels we  
199 added a step to control the overall volume of the template. We calculated the mean intracranial  
200 volume (ICV) of all the subjects in the cohort  $V_{\text{coh}}$ , and then calculated the volume of the initial  
201 mean-affine brain mask  $V_{\text{aff}}$ . The volume ratio  $r_{\text{vol}} = V_{\text{coh}}/V_{\text{aff}}$  was calculated, and each of the  
202 three dimensions of the mean-affine volume were scaled down by the appropriate length scaling  
203 factor  $r_{\text{vol}}^{1/3}$ . In this way, the final volume of the templating process retained a representative size  
204 for the cohort.

205 The next alignment stages were comprised of nonlinear registration using AFNI's 3dQwarp [Cox  
206 and Glen, 2013]. At each successive level the nonlinear alignment was performed to an increasingly  
207 higher refinement, resulting in mean volumes of greater detail. Specifically, nonlinear alignment at  
208 each stage was implemented to create mean templates as follows (A-E), using 3dQwarp's default  
209 "pcl" (Pearson correlation, clipped) cost function to reduce the effects of any outlier values (and  
210 unless otherwise specified, applying a 3D Gaussian blur):

211 A) **mean-NL0**: after registering to mean-affine with a minimum patch size of 101 mm and blurring

- 212 of 0 mm (base) and 9 mm (source);
- 213 B) **mean-NL1**: after registering to mean-NL0 with a minimum patch size of 49 mm and blurring
- 214 of 1 mm (base) and 6 mm (source);
- 215 C) **mean-NL2**: after registering to mean-NL1 with a minimum patch size of 23 mm and blurring
- 216 of 0 mm (base) and 4 mm (source);
- 217 D) **mean-NL3**: after registering to mean-NL2 with a minimum patch size of 13 mm and blurring
- 218 of 0 mm (base) and 2 mm median filter (source);
- 219 E) **mean-NL4**: after registering to mean-NL3 with a minimum patch size of 9 mm and blurring
- 220 of 0 mm (base) and 2 mm median filter (source).

221 Each mean-NL\* volume was resized in the same manner as the initial stages, although the correction

222 factors were much smaller here. Additionally, each intermediate mean-NL\* volume was anisotrop-

223 ically smoothed (preserving edges within the volume, for detail) using 3danissmooth, in order to

224 sharpen its contrast for subsequent alignments.

225 The mean-NL4 volume became the final group mean template for each cohort, as in all cases results

226 appeared to have essentially converged after this number of step. The coordinate system of this

227 mean volume defines the template space for that age group, and is labelled “IBT\_C1”, “IBT\_C2”,

228 etc.

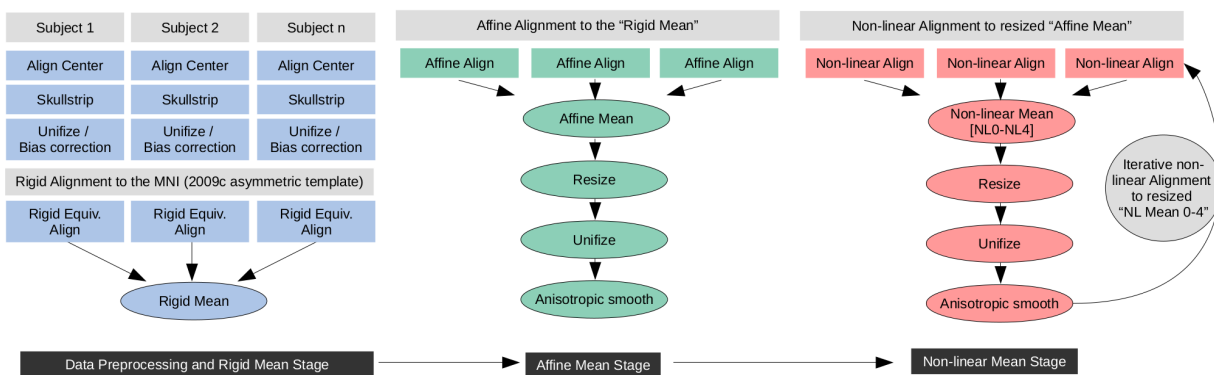


**Figure 1** – Schematic representation of the steps involved in the Dask pipeline (make\_template\_dask.py) for generating population-average brain templates.

## 229 2.5 “Typical” subject template generation

230 We used the following approach to find the maximally representative individual brain for the mean

231 template from the underlying cohort, in order to generate an additional “typical” template for that

232 space, in complement to the mean template.



233 To find the most typical subject for the mean template quantitatively, the lpa cost function value  
234 from aligning each subject’s anatomical to the final mean-NL4 was compared across the group; that  
235 is, the degree of similarity of each subject’s aligned volume to the mean template base was compared  
236 across the cohort. The individual brain in that mean template space with the lowest cost function  
237 value was selected to be the “typical template” brain. Alignment results were also visually verified  
238 for each typical template. We note that the typical template volume uses the same coordinate  
239 system as the mean template, and thus no additional “coordinate space” is created in this process.

## 240 **2.6 Atlas generation for mean and typical templates**

241 For each cohort, atlases were generated for each of the mean and typical templates based on  
242 FreeSurfer parcellation and segmentation maps<sup>1</sup>. By default, recon-all produces two maps of  
243 ROIs (including both cortical and subcortical GM, WM, ventricles, etc.): the “2000” map, using  
244 the Desikan-Killiany Atlas [Desikan et al., 2006] and the “2009” map, using the Destrieux Atlas  
245 [Destrieux et al., 2010]. Each of these maps was used to create a “2000” and “2009” atlas for each  
246 template.

247 For the mean template, maximum probability map (MPM) atlases were reconstructed as follows.  
248 The FreeSurfer parcellations for each subject were transformed to the IBT space using the warps  
249 created during the template creation process (and “nearest neighbor” interpolation, to preserve  
250 ROI identity). For a given parcellation, the fraction of overlap of a given ROI at each voxel in the  
251 template was computed. That overlap fraction is essentially the probability of a region to be mapped  
252 to that voxel. In this way, an MPM atlas was created for each of the 2000 and 2009 parcellations,  
253 labelled “IBT\_C1\_MPM\_2000”, “IBT\_C1\_MPM\_2009”, etc. The value of each voxel’s maximum  
254 probability was also kept and stored in a map, for reference and validation. Locations with max  
255 probability near 1 show greatest uniformity across group, and locations with lower values show  
256 greater variability.

257 For each typical template volume, atlases based on the 2000 and 2009 FreeSurfer parcellation were  
258 also created. First, the parcellations from original subject space were mapped to the individual  
259 template space. Then, each parcellation was passed through a modal smoothing process using  
260 3dLocalstat: for each voxel in the atlas, its value was reassigned to the mode of its NN=1 neigh-  
261 borhood (i.e., among “facewise” neighbors, so within a 7 voxel neighborhood). In this way the  
262 final atlas parcellation was slightly regularized, in order to reduce the effects of resampling to the  
263 template space. A typical brain atlas was created from each of the 2000 and 2009 parcellations,  
264 labelled “IBT\_C1\_TYP\_2000”, “IBT\_C1\_TYP\_2009”, etc.

---

<sup>1</sup>FreeSurfer distinguishes between cortical parcellations and subcortical segmentations; here, we use “parcellation” generically to refer to final map of all ROIs.

## 265 2.7 Validation and tests

266 The fractional volumes of each ROI in the MPM atlases were checked for being representative of  
267 each cohort. For this we calculated the logarithm of the relative volume ratio of each ROI:

$$r_i = \log \left( \frac{V_{\text{MPM},i} / V_{\text{MPM,ICV}}}{\frac{1}{N} \sum_j V_{j,i} / V_{j,\text{ICV}}} \right), \quad (1)$$

268 where the numerator is the fractional volume of a given  $i$ th ROI in the MPM (i.e., volume of the  
269 ROI divided by that template's ICV), and the denominator is the fractional volume of that  $i$ th  
270 ROI averaged across all  $N$  subjects (i.e., for each  $j$ th subject, volume of the ROI divided by the  
271 subject's ICV, in native space). Thus,  $r_i$  values close to 0 reflect high similarity of the MPM ROI  
272 to the cohort mean, and negative or positive values reflect a relative compression or expansion,  
273 respectively, of the MPM ROI relative to that for a particular cohort.

274 In order to quantify the inter-subject brain morphological variability for participants in each age-  
275 band, we calculated a region-wise mean deformation value (mDV) from the deformation warp fields  
276 generated during non-linear registration to the age-specific IBT. For this, the absolute warp value  
277 was summed across all three axes (L1-norm) and averaged across all the voxels within each ROI  
278 in the age-specific MPM atlas. A larger mDV indicates greater inter-subject brain morphological  
279 variability.

280 To examine the utility of the IBTs on a real, representative dataset, a separate sample of Indian  
281 population data was included for validation and testing purposes. For each cohort, the validation  
282 group ("V1", matched with cohort C1; "V2", matched with cohort C2; etc.) comprised 20 subjects  
283 within the corresponding age range. The T1w and resting state functional MRI (rs-fMRI) data  
284 acquisition information and demographics of these additional groups are provided in Supplementary  
285 Table ST1. For each IBT, in comparison to the MNI ICBM-152 template, the following validation  
286 tests were conducted using the T1w and resting functional data.

287 We first used the deformation field to characterize the difference between the two templates (IBT vs  
288 MNI). For each subject in the validation cohort, we calculated the absolute amount of displacement  
289 needed to move a voxel location from native space to the target in the new age-specific IBT and  
290 the standard MNI ICBM-152 templates, for non-linear registration. A median absolute distance  
291 along each axis (LR = left-right; PA = posterior-anterior; IS = inferior-superior) was calculated  
292 from the dimensional deformation field in each voxel. The median absolute distances when warping  
293 to MNI and cohort-specific IBT along each axis were compared using a paired sample Wilcoxon's  
294 signed-ranks test.

295 Finally, the practical benefits of using the IBT reference volumes were investigated by processing  
296 a validation cohort with resting state fMRI data using the same pipeline twice: once with the  
297 IBT mean template, and once with the standard MNI template. AFNI's `afni_proc.py` command  
298 was used to generate the full fMRI processing pipeline and the exact command is provided in  
299 the supplementary text. The whole brain average of temporal signal-to-noise ratio (TSNR) of the  
300 preprocessed smoothed data was compared when using the IBT and MNI ICBM 152 templates  
301 as targets. We additionally demonstrate the differences in the regional brain connectivity when  
302 using the IBT and MNI ICBM 152 templates as targets. For this analysis, averaged time series  
303 were extracted from a sphere of 5mm radius centered on the age-specific IBT MPM and MNI  
304 atlas-based coordinates (the regions are labelled as per Desikan-Killiany Atlas). The time series  
305 were correlated region by region for each subject across the length of the time series. For each  
306 age-group, the average pairwise correlations (Fisher  $Z$ -transformed Pearson  $r$  value) from IBT and  
307 MNI space were plotted and compared against a line with intercept=0 and slope=1, indicating a  
308 1:1 relationship in the regional brain connectivity between IBT and MNI dataset.

### 309 **3 Results**

310 The first part of the output consists of both “population average” and “typical” Indian brain tem-  
311 plates for five specific age-ranges: late-childhood (C1), adolescence (C2), young adulthood (C3),  
312 adulthood (C4) and late adulthood (C5) [see Table 1 for the age-ranges]. The second part of the  
313 output is a set four IBT atlases (IBTAs) for each age range: both an MPM and a typical subject  
314 version of each of the Desikan-Killiany (FreeSurfer’s “2000”) and Destrieux (FreeSurfer’s “2009”)   
315 atlases.

316 Figure 2 shows an example of the successive stages in the creation of the C1 IBT. Throughout  
317 the refinement, details become progressively clearer, with tissue contrast and feature identification  
318 increasing. Additionally, the variance decreases in the gray and white tissues with each stage.

319 Figure 3 shows an example of the IBT and IBTA outputs for the C3 group, displaying multiple slices  
320 in sagittal, coronal and axial views; in all cases, the population average template is underlaid. The  
321 top row shows a size comparison with the overlaid MNI template (shows as edges). In the second row,  
322 the “typical” template version is overlaid translucently, showing the very high degree of structural  
323 similarity between the two template versions. The bottom two rows show the MPM 2000 and 2009  
324 IBTAs. Similar outputs for other age groups are provided in the Supplementary Information, in  
325 Figures S1-S5.

### Templatizing stages: C1 group

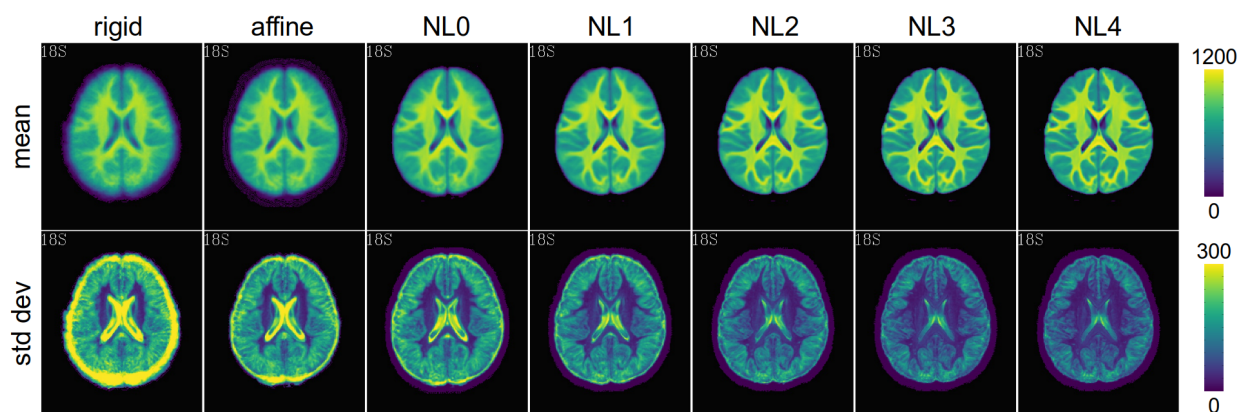


**Figure 2** – Axial slices of mean (top row) and standard deviation (bottom row) maps through successive stages of the templating algorithm (first stage at the left) for the C1 age-band. Note that the mean and standard deviation maps have separate scales, to show details more clearly in each.

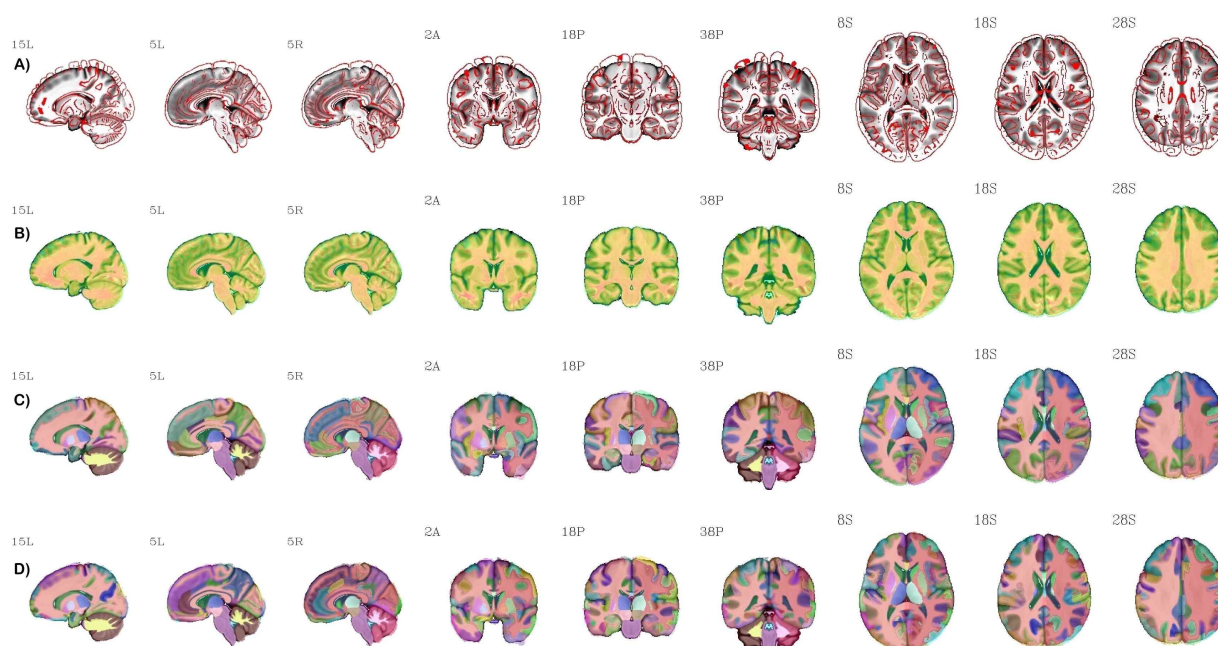


**Figure 3** – Three sets of sagittal, coronal and axial views of the “population-average” C3 IBT, displayed as underlay in grayscale in each row (A-D). Row A depicts the edge-filtered version of the MNI 2009 nonlinear template as overlay for size comparison. Row B shows the “typical” IBT C3 dataset as a translucent overlay; note the very high degree of structural similarity, as expected. The Indian MPM version of the DK atlas (FreeSurfer’s 2000 atlas) is shown in row C as overlay and Destrieux atlas (FreeSurfer’s 2009 atlas) as overlay in row D.

326 Figure 4's left panel displays the logarithm of the relative volume ratio of each ROI in the IBT MPM  
327 atlas (see Eq. (1)), showing how representative the atlas is of each cohort in a region-wise manner.  
328 As shown in the figure, most cortical regions have values close to zero, indicating that MPM ROIs  
329 in the IBT space provide representative volumes of the native space ROIs for each age group. The  
330 largest expansions were observed in the bilateral caudal and rostral middle frontal gyrus, bilateral  
331 rostral anterior cingulate, bilateral superior and inferior parietal cortices across the age groups.  
332 These are also the regions that show greater mDV (right-panel) indicating that greater inter-subject  
333 variability could be in part responsible for greater volumetric differences between native-space and  
334 MPM volumes. The scatter-plots in Supplementary Information (Figure S6) indicates that there  
335 were significant correlations between relative volume ratios and mDV for each age group ( $R$ -values:  
0.24-42 and  $p$ -values  $<0.05$  ).

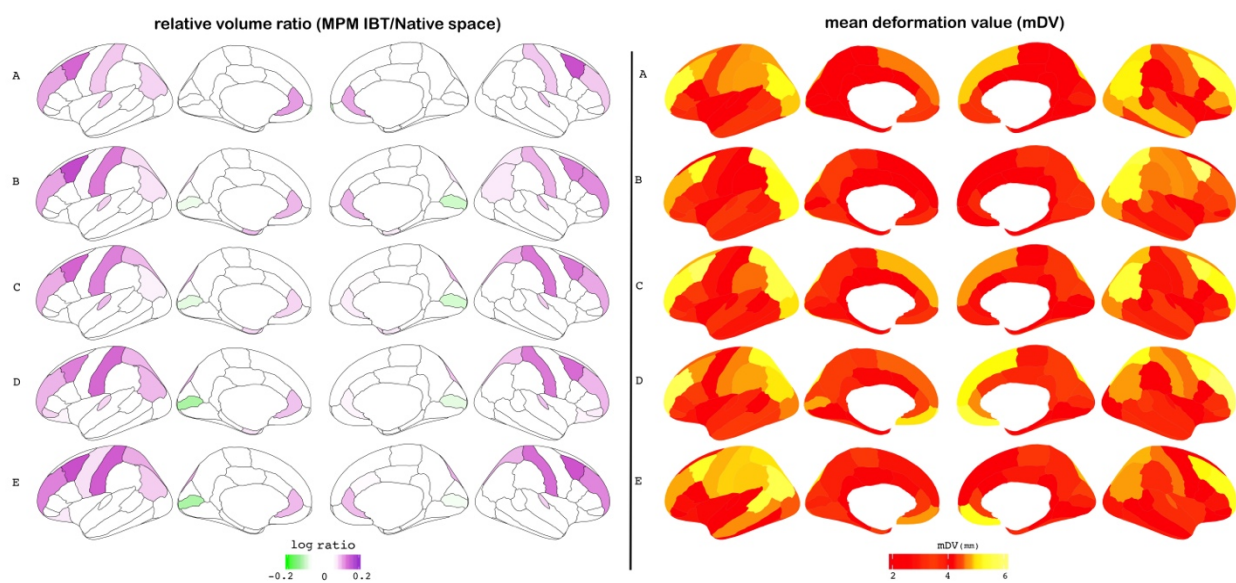


**Figure 4** – Evaluation of the region-wise similarity of the MPM volumes as measured (left panel) by the relative volume ratio for each ROI via Eq. (1), and (right panel) by mean deformation value (mDV) of each ROI; rows A-E show results for each age-specific group C1-C5, respectively. In the left-panel ROIs with notably different volume fractions are highlighted in purple (increases) and green (decreases), and in the right-panel ROIs with greater inter-subject variability are shown as increasingly yellow.

336

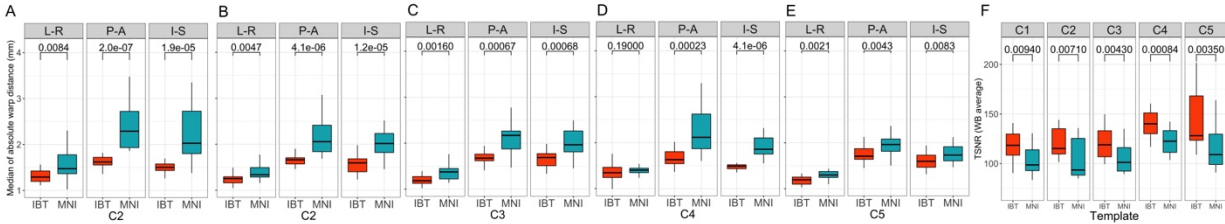


**Figure 5** – Validation cohort test results: (A-E) T1w-anatomical warping and (F) fMRI results, TSNR. IBT-based results are in orange, and MNI-based results in blue. Wilcoxon’s signed-ranks test was used to compare the distributions;  $p$ -values are shown at the top of each panel. For each validation group (V1-5), boxplots of the median warp magnitude along each major axis (LR, PA, IS) to a given template are shown in panel A-E. The warp distributions to MNI space are significantly larger along the AP and IS axes in all cases. While the differences tend to be smallest along the LR axis (particularly for C4), warps to MNI are nevertheless significantly larger for 4/5 of the cohorts along this axis, as well. Whole brain average TSNR (temporal signal-to-noise ratio) values from the processed output are displayed as boxplots in panel F. The average TSNR for the MNI normalization is significantly lower ( $p < 0.05$ , adjusted for  $N = 5$  multiple comparisons) in each case.

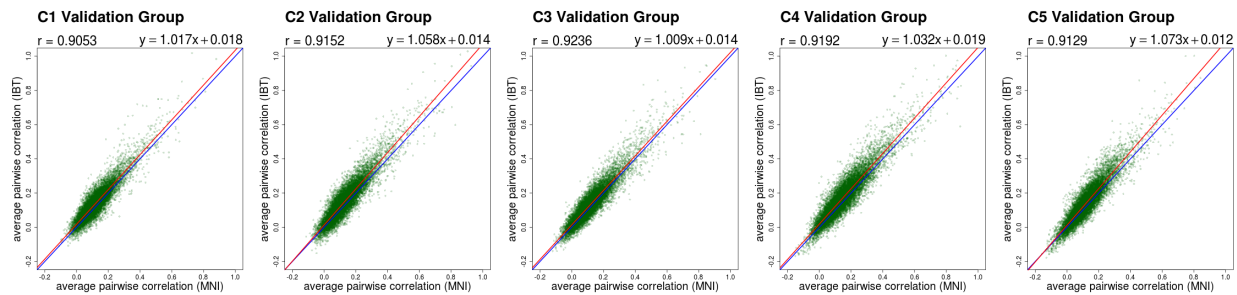


**Figure 6** – Validation cohort test results: fMRI results, FC. Comparisons of the average pairwise FC values in the IBT vs MNI space for each validation group. The blue line shows where a 1:1 relationship in the regional brain connectivity would be, and the red line represents the observed slope between IBT and MNI datasets. The correlations are similar, albeit slightly higher in the case of using the IBT template; this may be the result of slightly improved alignments on average, so that more similar time series are grouped together per ROI.

337 Figure 5A-E shows the comparison of warp distances from the anatomical (T1w) volumes of the  
 338 validation cohorts (V1-5) to each of the age-matched IBT “population mean” templates (orange),  
 339 vs the V1-5 warp distances to the standard MNI template (blue); for more detailed comparison,  
 340 average warp distances along each of the main volumetric axes are shown separately. In all cases,  
 341 alignment to an IBT dataset required much less overall displacement on average. Warps to MNI  
 342 were highly significantly greater ( $p < 0.05$ , corrected for  $N = 3 \times 5$  multiple comparisons) along the  
 343 PA and IS axes in all cases. Along the LR axes, differences were smaller but still significant at the  
 344 same level for 4/5 cohorts (again, warps to MNI being larger); the C4 cohort showed no significant  
 345 difference along the LR axis, but overall differences for this group were still large, due to the warps  
 346 along the other axes.

347 The results of using the IBT C1-5 datasets when processing fMRI data are shown for the validation  
348 cohorts in two comparisons. First, the average TSNR within the whole brain mask was higher  
349 for each cohort when warping to appropriate IBT as compared to using the MNI template (see  
350 Figure 5F). Second, Figure 6 displays scatterplots of functional connectivity (FC) values between  
351 corresponding ROI pairs when using either IBT or MNI space as a final template. The correlation  
352 of FC values is quite high in each case ( $r > 0.9$ ). However, the slopes were uniformly  $\gtrsim 1$ , indicating  
353 a small overall shift towards higher regional brain connectivity in the IBT space on average. This  
354 may reflect a better overall alignment to template space so that voxels are more appropriately  
355 grouped together (e.g., functional localization better matches anatomical parcellation, likely focused  
356 on boundaries between regions).

## 357 4 Discussion

358 We have introduced five new India brain template (IBTs) spaces, spanning an age range from 6-60  
359 years. Additionally, corresponding atlases (IBTAs) from widely used segmentations were also created  
360 for each space. These should form useful reference templates and region maps for brain imaging  
361 studies involving predominantly Indian populations. Both the creation of age-specific templates and  
362 the inclusion of associated atlases make the present study distinct from previous Indian population  
363 brain template projects [Rao et al., 2017, Bhalerao et al., 2018, Sivaswamy et al., 2019, Pai et al.,  
364 2020]; additionally, we have generated both “population mean” and high-contrast “typical” templates  
365 for each age band. The IBT volumes and corresponding atlases are publicly available for download,  
366 in standard NIFTI format, and freely usable by the wider neuroimaging community<sup>2</sup>.

367 The need for age-specific templates in particular has been recognized across different populations  
368 [Fonov et al., 2011, Wilke et al., 2002, Yoon et al., 2009]; however, Indian versions of age-specific  
369 brain templates have not been available to date. While adult brain templates may still provide  
370 reasonably accurate anatomical priors for normalizing lower resolution smoothed functional data,  
371 they may not be appropriate for high resolution structural and functional data [Wilke et al., 2002].  
372 For example, Yoon et al. [2009] examined the “template effect” in a pediatric population and noted  
373 significantly greater amount of deformation required for nonlinear normalization to the MNI152  
374 adult template than compared to an age-appropriate template (2.2 vs. 1.7 mm). Further, the  
375 authors also noted significant differences in both volume-based and surface-based morphological  
376 features between data warped to pediatric and adult brain templates. Such discrepancies are also  
377 reported in aging studies, where use of young-adult template (such as the MNI) for older adults can  
378 result in biases such as regional distortion and systematic over-expansion of older brains [Buckner

---

<sup>2</sup><https://doi.org/10.5281/zenodo.3817045>

379 [et al., 2004](#)]. Age-appropriate template for older adults have also been shown to provide more accu-  
380 rate tissue segmentation for structural imaging [[Fillmore et al., 2015](#)] and more focused activation  
381 patterns with improvement in sensitivity for fMRI group analyses [[Huang et al., 2010](#)].

382 In addition to age, consideration should also be given to the ethnic or population-specific differences  
383 [[Lee et al., 2005](#), [Tang et al., 2010](#), [Rao et al., 2017](#)], when choosing the appropriate brain template.  
384 As expected, there are noticeable structural differences when comparing the new IBTs with existing,  
385 popular standard templates (such as the MNI), which have been made from very different subject  
386 populations. Overall, registration to the IBTs from the Indian population validation groups required  
387 much less deformation of the input datasets and resulted in more accurate stereotactic standard-  
388 ization and anatomical localization. The relative differences in warping along the major axes of  
389 the brain were shown here using validation groups from the local population. The differences in  
390 warping magnitudes varied both by axis and by the age of subjects. Thus, the structural differences  
391 in templates are not trivial, i.e., just scaling, but instead reflect shape variations that are likely to  
392 significantly affect the overall goodness-of-fit and anatomical alignment across a group study.

393 Such aspects were highlighted in the differences of outcomes in fMRI processing when using IBT vs  
394 MNI templates: the IBT-based output tended to have higher SNR, and slightly higher FC values  
395 among ROI pairs. The latter fact in particular suggests that the IBTs provided better function-to-  
396 anatomical alignment across groups, so that voxel with functionally similar time series tended to be  
397 grouped together more preferentially. One might expect this to be a relatively small effect, because  
398 alignment to the MNI templates still appears generally reasonable; one would expect the overlap  
399 pattern differences to be occurring fractionally within ROIs and predominantly at boundaries. In-  
400 deed, the FC differences were relatively small, but with a noticeable trend toward higher values in  
401 the IBT-based datasets.

402 It is important to emphasize that these structural differences are only with regards to morphology;  
403 they do not relate to functional or behavioral outcomes, nor to intelligence, etc. The purpose and  
404 goal of population-specific templates is for the practical consideration of maximizing the matching  
405 of structures across a group during an alignment step of processing, as well as to better match  
406 functional regions to structures. These are geometric and signal-to-noise considerations, which are  
407 important in brain studies (as demonstrated here), but which are unrelated to the brain behavior  
408 itself.

409 The wide variety of brain structural patterns in any group, even in an apparently homogeneous  
410 one, is also worth commenting on. This inherent variability affects both the creation and utilization  
411 of brain templates [[Yang et al., 2020](#)]. In any population brain structures can vary to the degree  
412 of having different numbers of sulci in the same region (e.g., [[Thompson et al., 1996](#)] and *op cit*);  
413 this is true even in a group of controls who are highly localized, genetically related, similar age and



414 background, etc. Thus, there is a minimum and nontrivial degree of variability in alignment that  
415 one can reasonably expect both when combining multiple subjects to generate a template, as well as  
416 in the overlap of anatomical structures when applying the template. Indeed, the Indian population  
417 (currently over 1.3 billion people) is spread across a wide range of geographies with diversity in  
418 linguistic-ethnic compositions as well as extensive genetic admixtures [Basu et al., 2016]. In this  
419 study, the final mean template for each cohort contained variability. However, this was relatively  
420 low compared to the mean dataset values, and the final mean template contained a large amount of  
421 clearly defined structure. Moreover, the fractional overlap of ROIs when generating the maximum  
422 probability map atlases showed a high degree of agreement across the group through most of the  
423 brain.

424 The variability present in the template generation is also observable in the atlases. The inter-  
425 subject variability (as measured by the mean deformation values for various regions during non-linear  
426 registration to age and population-specific template) also correlated positively with the expansion  
427 of MPM volumes, in all age groups (see Supplementary Figure S6). While the final MPM atlases  
428 indicate the most frequent positions of each brain region in a given cohort, we also provide the  
429 probability density maps for each ROI in the atlas (see supplementary Figure S7 for example),  
430 which can be of additional use in ROI-based analyses.

431 While spatial normalization to IBT offers distinct advantages in terms of spatial accuracy and  
432 detection power, it may still be desirable to have the results from any particular analysis also  
433 reported in another space. For example, for comparisons with previously published studies, one  
434 might want to compare the locations of a finding with those reported in MNI, Talairach or Korean  
435 template coordinate spaces. Therefore, a nonlinear coordinate transformation mapping between  
436 IBT and the common MNI space has also been calculated, and a similar coordinate warp between  
437 *any* coordinate frames can be calculated easily.

438 There are several methodological strengths and limitations related to the current study that should  
439 be noted. We used combined state-of-the-art linear and non-linear averaging techniques using  
440 AFNI's completely automated pipeline "make\_template\_dask.py", which uses the Dask python  
441 parallelization to efficiently make a template from a large group of subjects. We addressed several  
442 specific challenges involved in the template creation, such as intensity normalization from different  
443 scanners, scaling, resizing of the overall brain size to be representative of the cohort at each iteration,  
444 and anisotropic smoothing with preservation of edges. While the overall sample size of the study  
445 was relatively large, the late childhood and the late adulthood templates had relative modest sample  
446 sizes. Therefore, it will be of benefit for the constructed templates to continue to be updated with  
447 larger sample sizes as we collect more MRI datasets. Future work should also expand the templates  
448 for ages  $< 6$  yr and  $> 60$  yr. We will also expand this work to include development of a cortical

449 surface atlas, which may allow for a registration procedure involving alignment of highly variable  
450 cortical folding patterns.

## 451 **5 Conclusions**

452 In conclusion, the present work demonstrates the appropriateness of using age and population-  
453 specific templates as reference targets for spatial normalization of structural and functional neu-  
454 roimaging data. This database of age-specific IBTs and IBTAs is made freely available to the wider  
455 neuroimaging community of researchers and clinicians worldwide. We hope that these tools will fa-  
456 cilitate research into neurological understand in general and into the functional and morphometric  
457 changes that occur over life-course in Indian population in particular.

### 458 **Highlights**

- 459 1. A new set of age-specific T1w Indian brain templates for ages 6-60 yr are developed and  
460 validated.
- 461 2. A new AFNI tool, `make_template_dask.py`, was developed for the creation of group-based  
462 templates
- 463 3. Maximum probability map atlases are also provided for each template.
- 464 4. Validation results indicate the appropriateness of Indian templates for spatial normalization  
465 of Indian brains

## 466 **Declaration of competing interest**

467 The authors have no financial or competing interests to declare.

## 468 **Author Contributions**

469 VB, RDB, BH, PAT and DRG conceptualized and designed the study. VB, RDB, PP, GV, UMM,  
470 JS, MK, KK, AC and DB contributed data to the study. BH, PAT, NV and DPO curated the  
471 data. BH and PAT conducted data quality assessments. BH, PAT, DRG and JAL conducted the  
472 computations required for template construction. GV and NPR contributed data for the validation  
473 experiments. BH and PAT conducted the validation experiments. BH and PAT took the lead in  
474 writing the manuscript. DRG, GJB, RDB, RWC and VB contributed to the interpretation of the  
475 findings and edited the manuscript for important intellectual content. All authors discussed the  
476 results and contributed to the final manuscript.

## 477 **Acknowledgments**

478 This work was partially supported by c-VEDA (Consortium on Vulnerability to Externalizing Disor-  
479 ders and Addictions) ICMR (India)/MRC (UK) (grant ICMR/MRC-UK/3/M/2015-NCD-I) to VB  
480 and GS. Wellcome Trust/DBT India Alliance Fellowship Grants to BH (Award: IA/RTF/14/1/1002),  
481 and UMM (Award: IA/E/12/1/500755), DST Research Grant SR/CSI/44/2008(5) to RDB and  
482 DBT Research Grant BT/PR14315/MED/30/474/2010 to PKP. GV acknowledges the support of  
483 the SwarnaJayanti Fellowship by the Department of Science and Technology, Government of In-  
484 dia (DST/SJF/LSA-02/2014–15). GS was supported by the Horizon 2020-funded ERC Advanced  
485 Grant ‘STRATIFY’ (brain network-based stratification of reinforcement-related disorders; 695313),  
486 ERANID (understanding the interplay between cultural, biological and subjective factors in drug  
487 use pathways; PR-ST-0416-10004), BRIDGET (JPND brain imaging, cognition, dementia and next  
488 generation GENomics; MR/N027558/1), the Human Brain Project (SGA 2, 785907, and SGA 3,  
489 945539), the National Institute of Health (NIH) (R01DA049238, A decentralized macro and mi-  
490 cro gene-by-environment interaction analysis of substance use behavior and its brain biomarkers).  
491 DRG, JAL, PAT and RWC were supported by the NIMH and NINDS Intramural Research Pro-  
492 grams (ZICMH002888) of the NIH (HHS, USA). This work utilized the computational resources of  
493 the NIH HPC Biowulf cluster (<http://hpc.nih.gov>).

## 494 References

- 495 Analabha Basu, Neeta Sarkar-Roy, and Partha P. Majumder. Genomic reconstruction of the history  
496 of extant populations of india reveals five distinct ancestral components and a complex structure.  
497 *Proceedings of the National Academy of Sciences*, 113(6):1594–1599, January 2016. doi: 10.1073/  
498 pnas.1513197113. URL <https://doi.org/10.1073/pnas.1513197113>.
- 499 G. V. Bhalerao, R. Parlikar, R. Agrawal, V. Shivakumar, S. V. Kalmady, N. P. Rao, S. M. Agarwal,  
500 J. C. Narayanaswamy, Y. C. J. Reddy, and G. Venkatasubramanian. Construction of population-  
501 specific indian mri brain template: Morphometric comparison with chinese and caucasian tem-  
502 plates. *Asian J Psychiatr*, 35:93–100, 2018. ISSN 1876-2026 (Electronic) 1876-2018 (Linking).  
503 doi: 10.1016/j.ajp.2018.05.014. URL <https://www.ncbi.nlm.nih.gov/pubmed/29843077>.
- 504 Randy L. Buckner, Denise Head, Jamie Parker, Anthony F. Fotenos, Daniel Marcus, John C. Morris,  
505 and Abraham Z. Snyder. A unified approach for morphometric and functional data analysis in  
506 young, old, and demented adults using automated atlas-based head size normalization: reliability  
507 and validation against manual measurement of total intracranial volume. *NeuroImage*, 23(2):724–  
508 738, October 2004. doi: 10.1016/j.neuroimage.2004.06.018. URL [https://doi.org/10.1016/j.](https://doi.org/10.1016/j.neuroimage.2004.06.018)  
509 [neuroimage.2004.06.018](https://doi.org/10.1016/j.neuroimage.2004.06.018).
- 510 R. W. Cox. Afni: software for analysis and visualization of functional magnetic resonance neuroim-  
511 ages. *Comput Biomed Res*, 29(3):162–73, 1996. ISSN 0010-4809 (Print) 0010-4809 (Linking). doi:  
512 10.1006/cbmr.1996.0014. URL <https://www.ncbi.nlm.nih.gov/pubmed/8812068>.
- 513 RW Cox and DR Glen. Nonlinear warping in afni. In *Poster presented at the 19th Annual Meeting*  
514 *of the Organization for Human Brain Mapping*, 2013.
- 515 Dask Development Team. *Dask: Library for dynamic task scheduling*, 2016. URL [https://dask.](https://dask.org)  
516 [org](https://dask.org).
- 517 R. S. Desikan, F. Segonne, B. Fischl, B. T. Quinn, B. C. Dickerson, D. Blacker, R. L. Buckner,  
518 A. M. Dale, R. P. Maguire, B. T. Hyman, M. S. Albert, and R. J. Killiany. An automated  
519 labeling system for subdividing the human cerebral cortex on mri scans into gyral based regions  
520 of interest. *Neuroimage*, 31(3):968–80, 2006. ISSN 1053-8119 (Print) 1053-8119 (Linking). doi:  
521 10.1016/j.neuroimage.2006.01.021. URL <https://www.ncbi.nlm.nih.gov/pubmed/16530430>.
- 522 Christophe Destrieux, Bruce Fischl, Anders Dale, and Eric Halgren. Automatic parcellation of  
523 human cortical gyri and sulci using standard anatomical nomenclature. *Neuroimage*, 53(1):1–15,  
524 2010. ISSN 1053-8119.
- 525 Alan C Evans, D Louis Collins, SR Mills, ED Brown, RL Kelly, and Terry M Peters. 3d statistical

- 526 neuroanatomical models from 305 mri volumes. In *1993 IEEE conference record nuclear science*  
527 *symposium and medical imaging conference*, pages 1813–1817. IEEE, 1993.
- 528 Paul T. Fillmore, Michelle C. Phillips-Meek, and John E. Richards. Age-specific MRI brain and head  
529 templates for healthy adults from 20 through 89 years of age. *Frontiers in Aging Neuroscience*, 7,  
530 April 2015. doi: 10.3389/fnagi.2015.00044. URL <https://doi.org/10.3389/fnagi.2015.00044>.
- 531 B. Fischl. Freesurfer. *Neuroimage*, 62(2):774–81, 2012. ISSN 1095-9572 (Electronic) 1053-  
532 8119 (Linking). doi: 10.1016/j.neuroimage.2012.01.021. URL [https://www.ncbi.nlm.nih.gov/  
533 pubmed/22248573](https://www.ncbi.nlm.nih.gov/pubmed/22248573).
- 534 V. Fonov, A. C. Evans, K. Botteron, C. R. Almli, R. C. McKinstry, D. L. Collins, and Group  
535 Brain Development Cooperative. Unbiased average age-appropriate atlases for pediatric studies.  
536 *Neuroimage*, 54(1):313–27, 2011. ISSN 1095-9572 (Electronic) 1053-8119 (Linking). doi: 10.1016/  
537 j.neuroimage.2010.07.033. URL <https://www.ncbi.nlm.nih.gov/pubmed/20656036>.
- 538 Chih-Mao Huang, Shwu-Hua Lee, Ing-Tsung Hsiao, Wan-Chun Kuan, Yau-Yau Wai, Han-Jung Ko,  
539 Yung-Liang Wan, Yuan-Yu Hsu, and Ho-Ling Liu. Study-specific EPI template improves group  
540 analysis in functional MRI of young and older adults. *Journal of Neuroscience Methods*, 189(2):  
541 257–266, June 2010. doi: 10.1016/j.jneumeth.2010.03.021. URL [https://doi.org/10.1016/j.  
542 jneumeth.2010.03.021](https://doi.org/10.1016/j.jneumeth.2010.03.021).
- 543 Jae Sung Lee, Dong Soo Lee, Jinsu Kim, Yu Kyeong Kim, Eunjoo Kang, Hyejin Kang, Keon Wook  
544 Kang, Jong Min Lee, Jae-Jin Kim, and Hae-Jeong Park. Development of korean standard brain  
545 templates. *Journal of Korean medical science*, 20(3):483–488, 2005. ISSN 1011-8934.
- 546 X. Li, P. S. Morgan, J. Ashburner, J. Smith, and C. Rorden. The first step for neuroimaging  
547 data analysis: Dicom to nifti conversion. *J Neurosci Methods*, 264:47–56, 2016. ISSN 1872-  
548 678X (Electronic) 0165-0270 (Linking). doi: 10.1016/j.jneumeth.2016.03.001. URL [https://  
549 www.ncbi.nlm.nih.gov/pubmed/26945974](https://www.ncbi.nlm.nih.gov/pubmed/26945974).
- 550 John Mazziotta, Arthur Toga, Alan Evans, Peter Fox, Jack Lancaster, Karl Zilles, Roger Woods,  
551 Tomas Paus, Gregory Simpson, Bruce Pike, et al. A four-dimensional probabilistic atlas of the  
552 human brain. *Journal of the American Medical Informatics Association*, 8(5):401–430, 2001a.
- 553 John Mazziotta, Arthur Toga, Alan Evans, Peter Fox, Jack Lancaster, Karl Zilles, Roger Woods,  
554 Tomas Paus, Gregory Simpson, Bruce Pike, et al. A probabilistic atlas and reference system for  
555 the human brain: International consortium for brain mapping (icbm). *Philosophical Transactions*  
556 *of the Royal Society of London. Series B: Biological Sciences*, 356(1412):1293–1322, 2001b.
- 557 Praful P. Pai, Pravat K. Mandal, Khushboo Punjabi, Deepika Shukla, Anshika Goel, Shallu Joon,  
558 Saurav Roy, Kanika Sandal, Ritwick Mishra, and Ritu Lahoti. BRAHMA: Population specific t1,

559 t2, and FLAIR weighted brain templates and their impact in structural and functional imaging  
560 studies. *Magnetic Resonance Imaging*, 70:5–21, July 2020. doi: 10.1016/j.mri.2019.12.009. URL  
561 <https://doi.org/10.1016/j.mri.2019.12.009>.

562 N. P. Rao, H. Jeelani, R. Achalia, G. Achalia, A. Jacob, R. D. Bharath, S. Varambally, G. Venkata-  
563 subramanian, and K. Yalavarthy P. Population differences in brain morphology: Need for  
564 population specific brain template. *Psychiatry Res Neuroimaging*, 265:1–8, 2017. ISSN 1872-  
565 7506 (Electronic) 0925-4927 (Linking). doi: 10.1016/j.psychresns.2017.03.018. URL <https://www.ncbi.nlm.nih.gov/pubmed/28478339>.

567 Z. S. Saad, D. R. Glen, G. Chen, M. S. Beauchamp, R. Desai, and R. W. Cox. A new method for  
568 improving functional-to-structural mri alignment using local pearson correlation. *Neuroimage*, 44  
569 (3):839–48, 2009. ISSN 1095-9572 (Electronic) 1053-8119 (Linking). doi: 10.1016/j.neuroimage.  
570 2008.09.037. URL <https://www.ncbi.nlm.nih.gov/pubmed/18976717>.

571 Eesha Sharma, Nilakshi Vaidya, Udita Iyengar, Yuning Zhang, Bharath Holla, Meera Purushottam,  
572 Amit Chakrabarti, Gwen Sascha Fernandes, Jon Heron, Matthew Hickman, Sylvane Desrivieres,  
573 Kamakshi Kartik, Preeti Jacob, Madhavi Rangaswamy, Rose Dawn Bharath, Gareth Barker,  
574 Dimitri Papadopoulos Orfanos, Chirag Ahuja, Pratima Murthy, Sanjeev Jain, Mathew Vargh-  
575 ese, Deepak Jayarajan, Keshav Kumar, Kandavel Thennarasu, Debashish Basu, B. N. Sub-  
576 odh, Rebecca Kuriyan, Sunita Simon Kurpad, Kumaran Kalyanram, Ghattu Krishnaveni, Mu-  
577 rali Krishna, Rajkumar Lenin Singh, L. Roshan Singh, Kartik Kalyanram, Mireille Toledano,  
578 Gunter Schumann, Vivek Benegal, and The cVEDA Consortium. Consortium on vulnerabil-  
579 ity to externalizing disorders and addictions (cveda): A developmental cohort study proto-  
580 col. *BMC Psychiatry*, 20(1):2, 2020. ISSN 1471-244X. doi: 10.1186/s12888-019-2373-3. URL  
581 <https://doi.org/10.1186/s12888-019-2373-3>.

582 J. Sivaswamy, A. J. Thottupattu, R. Mehta, R. Sheelakumari, and C. Kesavadas. Construction  
583 of indian human brain atlas. *Neurol India*, 67(1):229–234, 2019. ISSN 0028-3886 (Print) 0028-  
584 3886 (Linking). doi: 10.4103/0028-3886.253639. URL <https://www.ncbi.nlm.nih.gov/pubmed/30860125>.

586 Jean Talairach and Pierre Tournoux. Co-planar stereotaxic atlas of the human brain-3-dimensional  
587 proportional system. *An approach to cerebral imaging*, 1988.

588 Y. Tang, C. Hojatkashani, I. D. Dinov, B. Sun, L. Fan, X. Lin, H. Qi, X. Hua, S. Liu, and A. W.  
589 Toga. The construction of a chinese mri brain atlas: a morphometric comparison study between  
590 chinese and caucasian cohorts. *Neuroimage*, 51(1):33–41, 2010. ISSN 1095-9572 (Electronic)  
591 1053-8119 (Linking). doi: 10.1016/j.neuroimage.2010.01.111. URL <https://www.ncbi.nlm.nih.gov/pubmed/20152910>.

- 593 P. M. Thompson, C. Schwartz, R. T. Lin, A. A. Khan, and A. W. Toga. Three-dimensional statistical  
594 analysis of sulcal variability in the human brain. *J Neurosci*, 16(13):4261–74, 1996. ISSN 0270-  
595 6474 (Print) 0270-6474 (Linking). URL <https://www.ncbi.nlm.nih.gov/pubmed/8753887>.
- 596 M. Wilke, V. J. Schmithorst, and S. K. Holland. Assessment of spatial normalization of whole-brain  
597 magnetic resonance images in children. *Hum Brain Mapp*, 17(1):48–60, 2002. ISSN 1065-9471  
598 (Print) 1065-9471 (Linking). doi: 10.1002/hbm.10053. URL [https://www.ncbi.nlm.nih.gov/  
599 pubmed/12203688](https://www.ncbi.nlm.nih.gov/pubmed/12203688).
- 600 Guoyuan Yang, Sizhong Zhou, Jelena Bozek, Hao-Ming Dong, Meizhen Han, Xi-Nian Zuo, Hesheng  
601 Liu, and Jia-Hong Gao. Sample sizes and population differences in brain template construction.  
602 *NeuroImage*, 206:116318, February 2020. doi: 10.1016/j.neuroimage.2019.116318. URL [https:  
603 //doi.org/10.1016/j.neuroimage.2019.116318](https://doi.org/10.1016/j.neuroimage.2019.116318).
- 604 U. Yoon, V. S. Fonov, D. Perusse, A. C. Evans, and Group Brain Development Cooperative. The  
605 effect of template choice on morphometric analysis of pediatric brain data. *Neuroimage*, 45(3):  
606 769–77, 2009. ISSN 1095-9572 (Electronic) 1053-8119 (Linking). doi: 10.1016/j.neuroimage.2008.  
607 12.046. URL <https://www.ncbi.nlm.nih.gov/pubmed/19167509>.
- 608 Y. Zhang, N. Vaidya, U. Iyengar, E. Sharma, B. Holla, C. K. Ahuja, G. J. Barker, D. Basu, R. D.  
609 Bharath, A. Chakrabarti, S. Desrivieres, P. Elliott, G. Fernandes, A. Gourisankar, J. Heron,  
610 M. Hickman, P. Jacob, S. Jain, D. Jayarajan, K. Kalyanram, K. Kartik, M. Krishna, G. Kr-  
611 ishnaveni, K. Kumar, K. Kumaran, R. Kuriyan, P. Murthy, D. P. Orfanos, M. Purushottam,  
612 M. Rangaswamy, S. S. Kupard, L. Singh, R. Singh, B. N. Subodh, K. Thennarasu, M. Toledano,  
613 M. Varghese, V. Benegal, G. Schumann, and Veda consortium c. The consortium on vulnerability  
614 to externalizing disorders and addictions (c-veda): an accelerated longitudinal cohort of children  
615 and adolescents in india. *Mol Psychiatry*, 2020. ISSN 1476-5578 (Electronic) 1359-4184 (Linking).  
616 doi: 10.1038/s41380-020-0656-1. URL <https://www.ncbi.nlm.nih.gov/pubmed/32203154>.

## 617 Supplementary Information

618 This section provides supplementary figures and codes to the material in the main text.

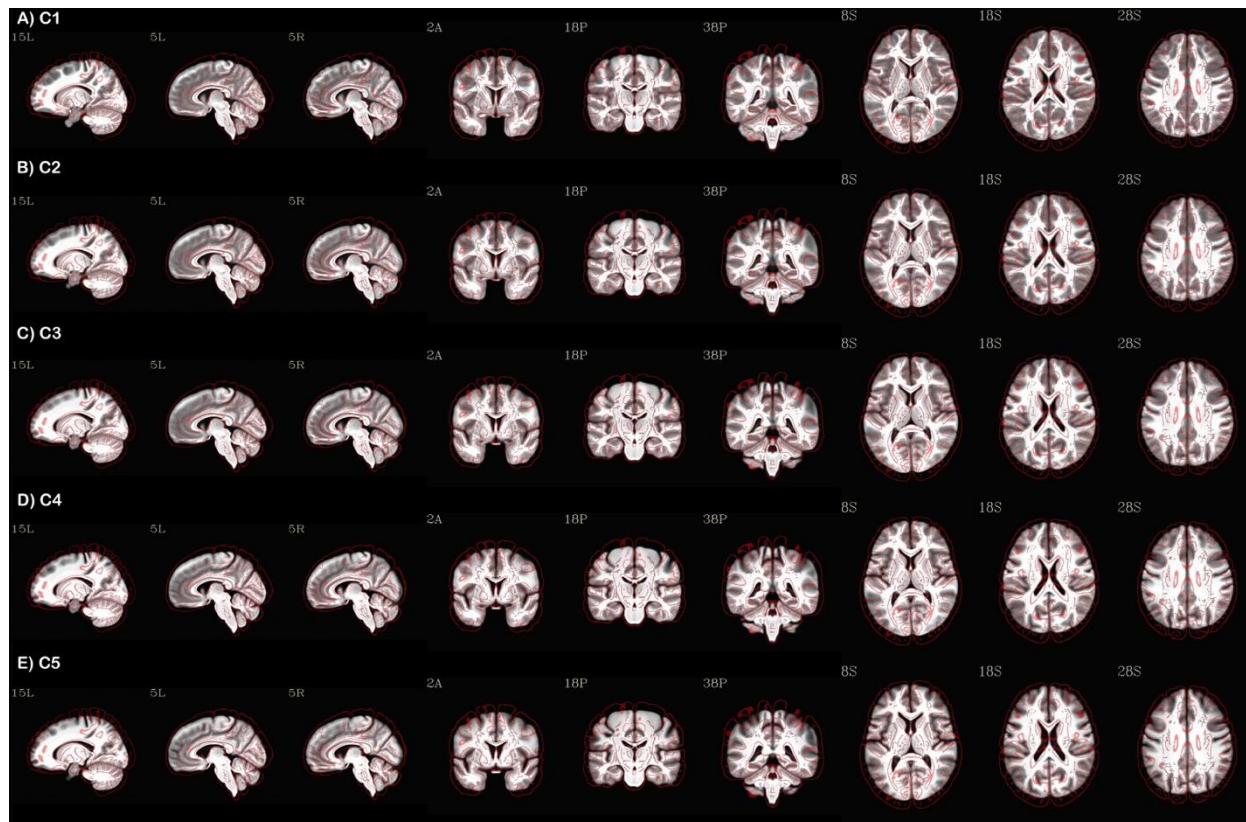


**Figure S1** – The five IBTs (C1-5) with three sets of sagittal, coronal and axial view displayed as underlay in grayscale and edge-filtered version of the MNI 2009 non-linear template mask as overlay for size comparison. High tissue contrast and detail are evident in each case.



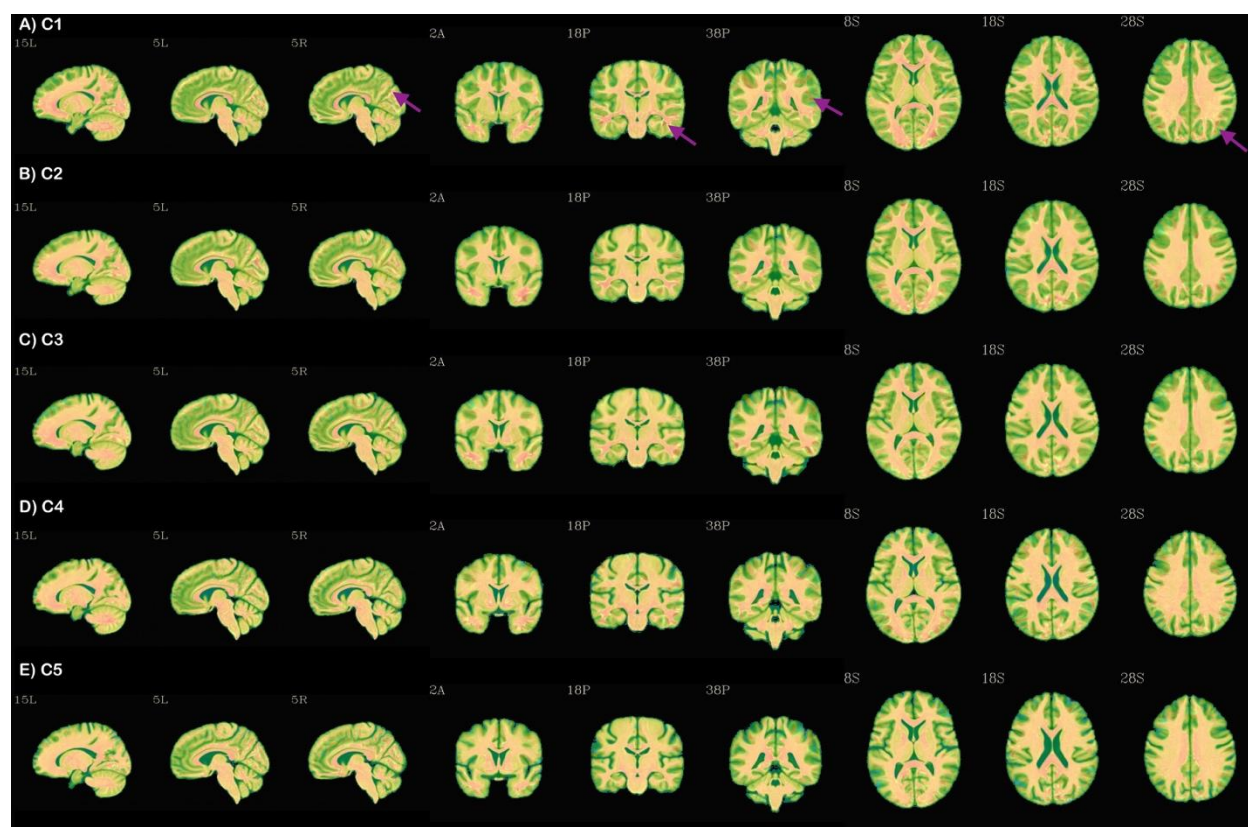


**Figure S2** – The five population-average IBTs (C1-5) with three sets of sagittal, coronal and axial view displayed as underlay in grayscale and the respective typical subject for each IBT version as the overlay. Arrow points to example regions in C1 age-band regions where the typical version provides greater details than the underlying population-average version.

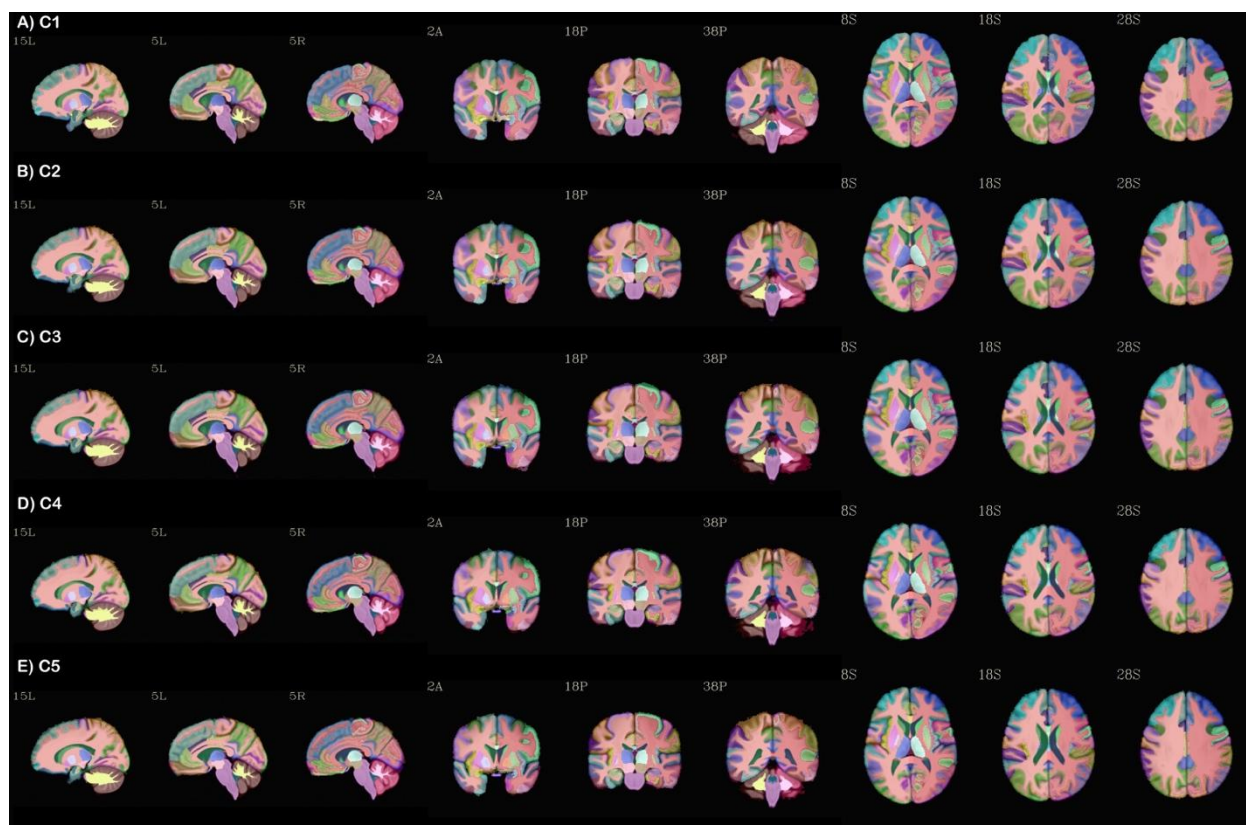


**Figure S3** – The five IBTs (C1-5) with three sets of sagittal, coronal and axial view displayed as underlay in grayscale and the respective Indian maximum probability map version of the DK atlas (FreeSurfer's 2000 Atlas) as overlay in AFNI's "ROI\_i256" color scale.

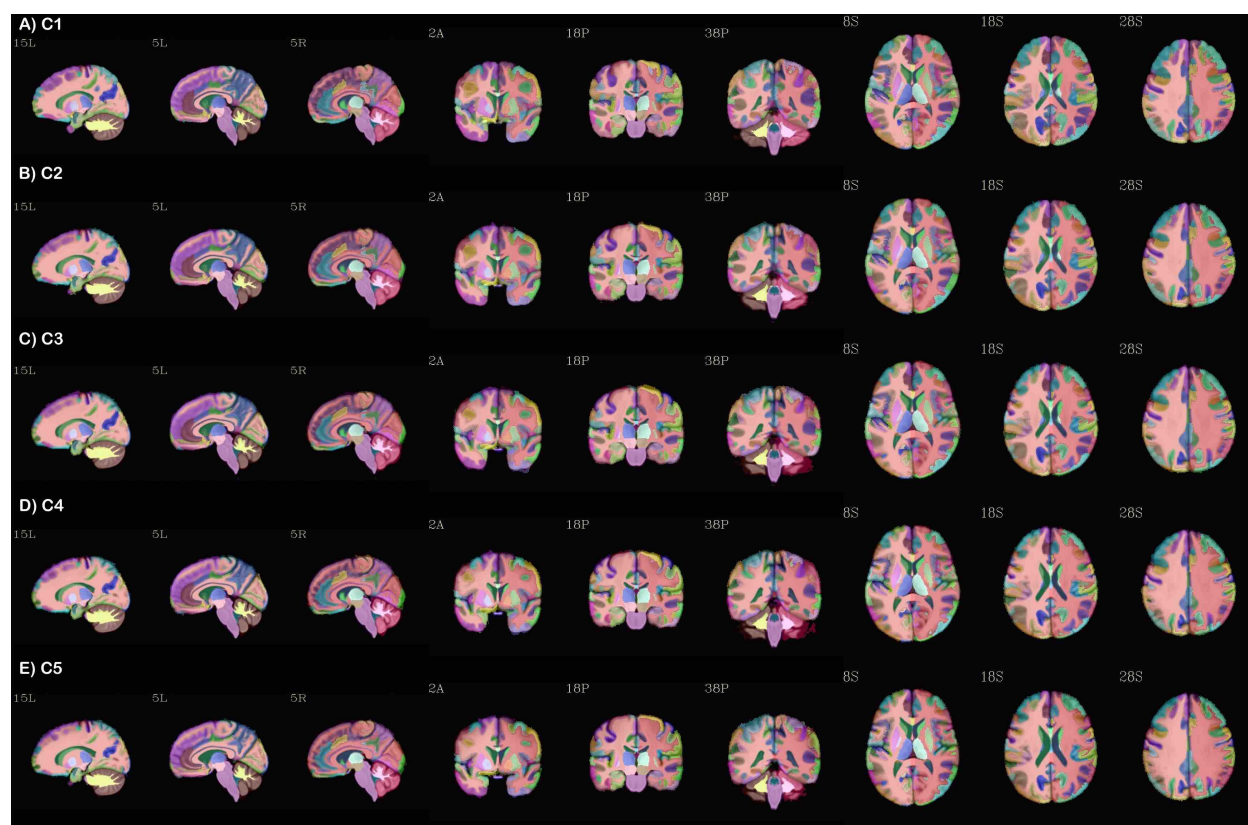


**Figure S4** – The five IBTs (C1-5) with three sets of sagittal, coronal and axial view displayed as underlay in grayscale and the respective Indian maximum probability map version of the Destrieux atlas (FreeSurfer’s 2009 Atlas) as overlay in AFNI’s “ROI\_i256” color scale.

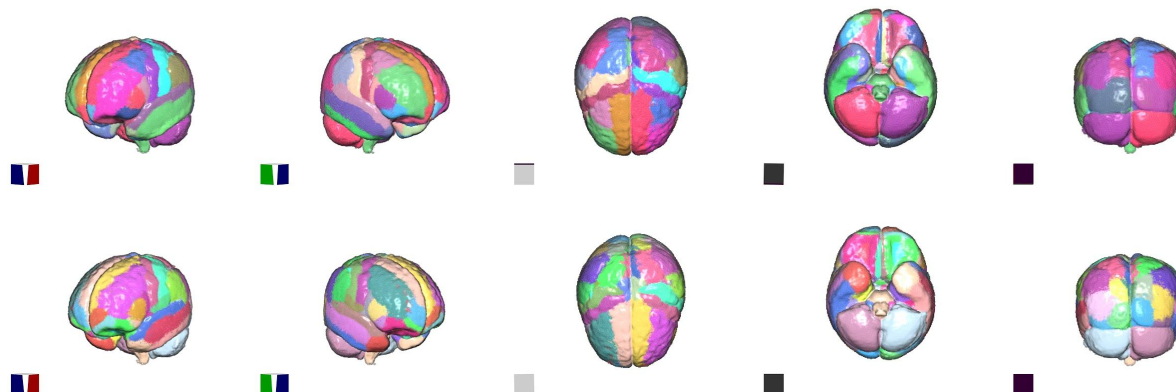


**Figure S5** – 3D surface view of the brain atlases for the C1-IBT age band. The top row shows the maximum probability map (MPM) version of the DK atlas (FreeSurfer's 2000 Atlas) and the bottom row shows MPM version of the Destrieux atlas (FreeSurfer's 2009 Atlas) for the C1 age band.

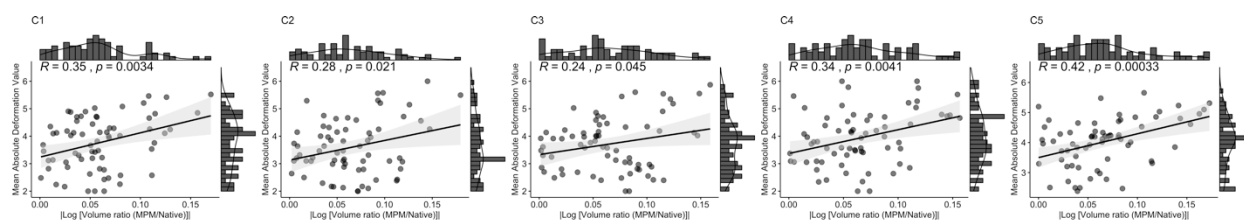


**Figure S6** – Scatterplot with marginal densigram for pairwise correlations between absolute values of logarithm of the relative volume ratios and mean absolute deformation value across all the regions in the maximum probability map (MPM) version of the DK atlas (FreeSurfer's 2000 Atlas) at each age-group C1-C5.

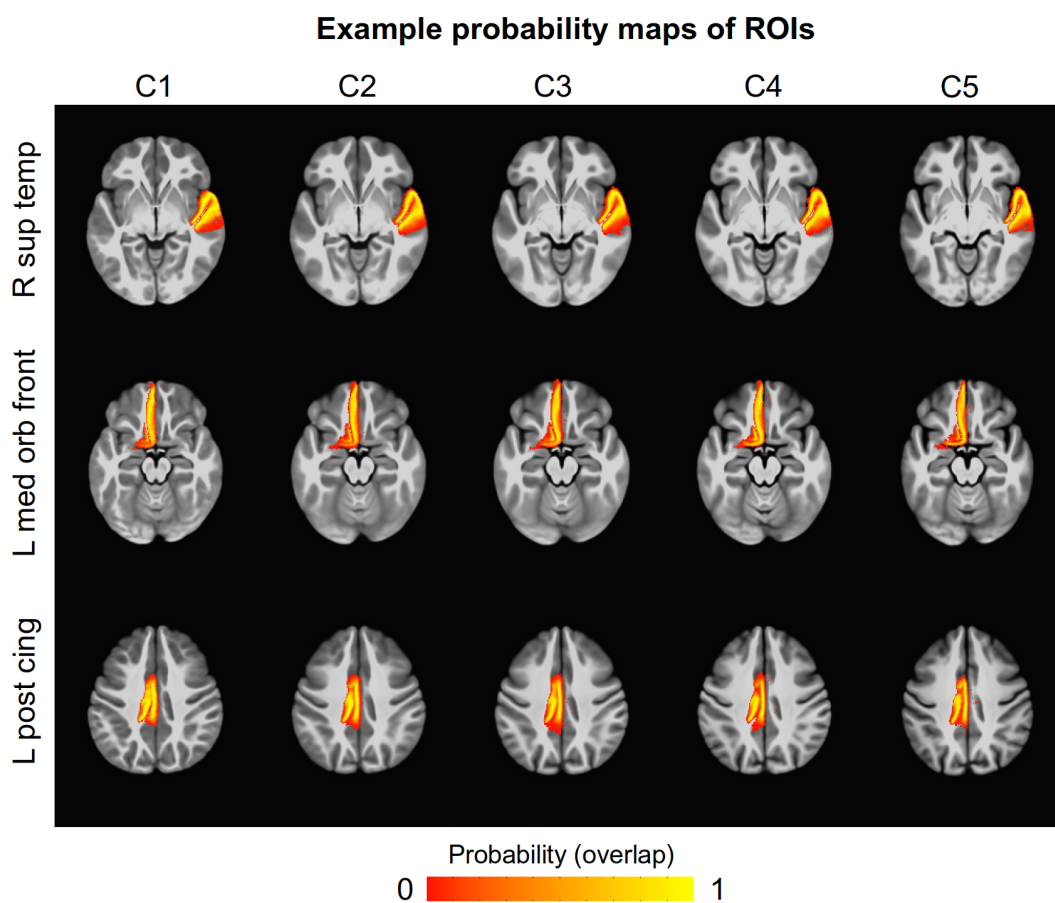


**Figure S7** – Axial views for three example region of interest from MPM-2000 IBT atlas for all the age groups. The top row shows probability map for right superior temporal gyrus, middle row shows left medial orbital frontal gyrus and the bottom row shows left posterior cingulate gyrus. The color intensity reflects probability density estimates (ranging from 0 to 1)

619 **Supplementary Information:** Example afni\_proc.py command for comparing validation tests.

```
620 #!/bin/bash
621
622 sub=$1 # subject ID;
623 dir=$2 # output directory
624
625 afni_proc.py \
626     -subj_id ${sub} \
627     -out_dir ${dir} \
628     -blocks despike tshift align tlrc volreg blur mask regress \
629     -copy_anat anatSS.${sub}.nii \
630     -anat_has_skull no \
631     -dsets ${sub}_rest.nii.gz \
632     -tcats_remove_first_trs 10 \
633     -align_opts_aea -ginormous_move -deoblique on -cost lpc+ZZ \
634     -volreg_align_to MIN_OUTLIER \
635     -volreg_align_e2a \
636     -volreg_tlrc_warp \
637     -tlrc_base C1_IBT_SSW.nii.gz \
638     -tlrc_NL_warp \
639     -tlrc_NL_warped_dsets \
640     anatQQ.${sub}.nii \
641     anatQQ.${sub}.aff12.1D \
642     anatQQ.${sub}_WARP.nii \
643     -volreg_warp_dxyz 3 \
644     -mask_segment_anat yes \
645     -regress_censor_outliers 0.2 \
646     -regress_apply_mot_types demean deriv \
647     -regress_est_blur_errts \
648     -regress_bandpass 0.01 0.2 \
649     -html_review_style pythonic \
650     -execute
```